

# Fast, faithful, frequency-domain effective-one-body waveforms for compact binary coalescences

Rossella Gamba<sup>1</sup>, Sebastiano Bernuzzi<sup>1</sup>, and Alessandro Nagar<sup>2,3,4</sup>

<sup>1</sup>*Theoretisch-Physikalisches Institut, Friedrich-Schiller-Universität Jena, 07743, Jena, Germany*

<sup>2</sup>*Centro Fermi - Museo Storico della Fisica e Centro Studi e Ricerche Enrico Fermi, Rome, Italy*

<sup>3</sup>*INFN Sezione di Torino, Via P. Giuria 1, 10125 Torino, Italy and*

<sup>4</sup>*Institut des Hautes Etudes Scientifiques, 91440 Bures-sur-Yvette, France*

(Dated: December 2, 2020)

The inference of binary neutron star properties from gravitational-wave observations requires the generation of millions of waveforms, each one spanning about three order of magnitudes in frequency range. Thus, waveform models must be efficiently generated and, at the same time, be faithful from the post-Newtonian quasi-adiabatic inspiral up to the merger regime. A simple solution to this problem is to combine effective-one-body waveforms with the stationary phase approximation to obtain frequency-domain multipolar approximants valid from any low frequency to merger. We demonstrate that effective-one-body frequency-domain waveforms generated in post-adiabatic approximation are computationally competitive with current phenomenological and surrogate models, (virtually) arbitrarily long, and faithful up to merger for any binary parameter. The same method can also be used to efficiently generate intermediate mass binary black hole inspiral waveforms detectable by space-based interferometers.

Gravitational-wave (GW) analyses of binary neutron star (BNS) signals rely on matched filtering techniques and waveform models to infer the source properties from observations. The inspiral-to-merger signal is observable in the ground-based interferometer frequency band for minutes, that correspond to thousands of inspiralling cycles to merger [1, 2]. Waveform templates must model the signal phase evolution over a frequency range spanning from few Hz to kHz [3–5]. Further, due to the large number ( $\sim 10^7$ ) of waveforms needed to explore the posterior distribution of the parameters, such models also need to be computationally efficient. Similar issues arise for the computation of waveforms for binary black hole (BBH) inspirals, that are observable in the mHz to Hz and dHz regime with space-based interferometers for binary masses  $\sim (100-10^5)M_\odot$  [6–8]. In this case, the waveforms efficiency requirements are even more demanding as the binary remains in band for days to years, corresponding to up to millions inspiralling cycles [9].

Analytical post-newtonian (PN) approximants are quick to evaluate and can be turned into closed-form frequency-domain templates by applying the stationary phase approximation (SPA) [10–14]. While PN approximants become unfaithful as the binary motion becomes nonadiabatic (high velocities regime), the domain of validity of the SPA itself was proven to be accurate at least up to frequencies corresponding to the last stable orbit, e.g. [11, 13]. Such a validity interval corresponds to binaries with total mass  $M \lesssim 13M_\odot$  in the ground-based interferometers range, and it is large enough to cover BNS and - possibly - also light BHNS or BBH systems. From the trivial scaling of the waveform with the binary mass, it follows that the validity of the SPA holds also for the inspiral of stellar and intermediate-mass BBH [6, 7].

Beyond PN approximants, effective-one-body

(EOB) [15–27] and phenomenological (Phenom) [28–33] models describe the waveform from the early inspiral up to merger [and ringdown, if dealing with BBH systems], but are in general computationally less efficient. While Phenom models output frequency domain (FD) waveforms, EOB models natively generate time domain (TD) waveforms, so that an additional Fourier transform is needed, with the related performance loss. Reduced-order modeling techniques offer a solution to the issue of performances as they can be used to produce fast surrogate models from a training set of waveforms [34–38]. However, surrogate waveforms are limited by the length and parameters span of the training set and they must be regenerated if the baseline model is varied.

EOB waveforms can alternatively be speeded up using dedicated analytical methods. The postadiabatic method gives an approximate, iterative solution for the EOB (circular) Hamiltonian dynamics [39–41]. Such a simple, physically motivated technique was shown to allow for the computation of BNS TD waveforms from frequencies as low as a few Hz in a matter of tens of milliseconds. However, such waveforms still need to be translated in the FD. In this work we apply the SPA to EOB waveforms in order to obtain computationally inexpensive frequency-domain templates. The FD waveforms obtained this way are suitable for the GW data analysis of BNS signal up to merger and of long BBH inspiral for masses  $\gtrsim 1000M_\odot$ . Throughout this work  $M$  is the binary mass,  $q \geq 1$  the mass ratio,  $m_i$  ( $i = 1, 2$ ) the individual masses,  $\nu = m_1 m_2 / M^2$ ,  $\chi_i \equiv S_i / m_i^2$  the dimensionless individual spins (anti)aligned with the orbital angular momentum,  $\Lambda_i$  the individual quadrupolar tidal polarizability parameters [42–45], and  $\tilde{\Lambda}$  the reduced tidal parameter [46–48]. Geometric units  $G = c = 1$  are

employed unless stated differently.

The FD extension of a given a TD EOB waveform is computed by applying the SPA to the multipolar TD modes  $h_{\ell m}(t) = a_{\ell m} e^{i\phi_{\ell m}(t)}$  to obtain

$$\tilde{h}_{\ell m}^{\text{SPA}} = \tilde{A}_{\ell m}^{\text{SPA}} e^{i\psi_{\ell m}^{\text{SPA}}} = \frac{a_{\ell m}(t_f)}{\sqrt{\ddot{\phi}_{\ell m}(t_f)/2\pi}} e^{i[\psi_f(t_f^{\ell m}) - \pi/4]}, \quad (1)$$

with  $\psi_f(t) \equiv 2\pi ft - \phi(t)$  and where  $t_f$  denotes the saddle point of  $\psi_f(t)$ . The two GW polarizations in FD are then computed by combining the multipolar modes with spin-weighted spherical harmonics in a standard way. The TD-to-FD computation is straightforward, the key technical details in our implementations are given in the Supplemental Material. We apply the SPA to TD `TEOBResumS`, a state-of-the-art effective EOB approximant for spin-aligned binaries [26, 41, 49–52], that includes resummed tidal interactions from PN and gravitational-self force results [40, 41, 53]. We shall show that the FD `TEOBResumSPA` retains the same accuracy as the TD `TEOBResumS` up to merger for any BNS signal, and that for waveforms with initial frequency  $f_0 \lesssim 15$  Hz its speed is comparable to `SEOBNRv4Tsurrogate`.

Figure 1 (left panel) shows the FD phasing of a fiducial BNS waveform for a  $(M/M_\odot, q, \chi_1, \chi_2, \tilde{\Lambda}) = (2.8, 1, 0, 0, 400)$  system, sampled at 8192 Hz with initial frequency  $f_0 = 20$  Hz and computed either Fourier transforming the TD `TEOBResumS` (solid black line) or using the SPA (dashed red line). `TEOBResumSPA` correctly reproduces the waveform of the original TD model from the early inspiral up to merger; the accumulated total phase difference amounts to  $\sim 0.1$  to merger (vertical line).

We quantitatively assess the faithfulness of `TEOBResumSPA` against `TEOBResumS` on a sample of  $10^4$  waveforms from BNS with  $m_{1,2} \in [1, 2.5]M_\odot$ ,  $\chi_{1,2} \in [-0.5, +0.5]$  and  $\Lambda_{1,2} \in [10, 5000]$ . Since the masses and the tidal parameters are sampled separately, no specific equation of state is imposed. We recall that the mismatch  $\bar{\mathcal{F}}$  (and the match  $\mathcal{F}$ ) between two waveforms  $(h, s)$  is defined by

$$\bar{\mathcal{F}} \equiv 1 - \mathcal{F} = 1 - \max_{t_c, \phi_c} \frac{(h, s)}{\sqrt{(h, h)(s, s)}}, \quad (2)$$

where  $t_c$  and  $\phi_c$  denote the time and phase at coalescence, and the Wiener scalar product associated to the power-spectral density (PSD) of the detector,  $S_n(f)$ , is

$$(h, s) = 4 \Re \int \frac{\tilde{h}^*(f)\tilde{s}(f)}{S_n(f)} df. \quad (3)$$

Since the detection rate loss scales as  $(1 - (1 - \bar{\mathcal{F}})^3)$ ,  $\bar{\mathcal{F}} \leq 0.035$  is usually regarded to be satisfactory for detection purposes [54]. However, the value of  $\bar{\mathcal{F}}$  does not depend on the signal SNR and does not account properly for statistical fluctuations (or lack thereof) due to the

background noise. Two waveforms are faithful if [54–56]

$$\bar{\mathcal{F}} \leq \bar{\mathcal{F}}_{\text{SNR}} \equiv \frac{D}{2 \text{SNR}^2}, \quad (4)$$

where  $D = 6$  is the number of intrinsic parameters. This means that we require for the systematical errors introduced by the SPA approximation to be smaller than the expected statistical fluctuations. The threshold SNRs chosen in Eq. (4) are 13, 33 and 80. The first two values mimic the SNRs of the two BNSs observed by LIGO/Virgo in O3 and O2 respectively, while the last value can be reached for GW170817-like event at design sensitivity or in third generation detectors [57]. The above numbers lead to the threshold unfaithfulnesses of  $\bar{\mathcal{F}}_{13} \approx 1.8 \times 10^{-2}$ ,  $\bar{\mathcal{F}}_{33} \approx 2.7 \times 10^{-3}$  and  $\bar{\mathcal{F}}_{80} \approx 5 \times 10^{-4}$ .

Figure 1 (right panel) shows the matches between `TEOBResumS` and `TEOBResumSPA` for our BNS sample with a starting frequency  $f_0 = 20$  Hz and assuming the Advanced LIGO `ZeroDetunedHighPower` PSD [58]. We find that more than 99% of total mismatches lie below the most conservative threshold  $\bar{\mathcal{F}}_{80}$ . The worst performances ( $\bar{\mathcal{F}} \sim 5.2 \times 10^{-4}$  and  $\bar{\mathcal{F}} \sim 5.4 \times 10^{-4}$ ) are obtained for two cases with equal mass configurations and large  $\tilde{\Lambda}$  values ( $\tilde{\Lambda} > 2000$ ).

While the loss of accuracy with respect to the TD EOB is negligible, the speed up given by the SPA is significant. The computational performance of our FD EOB waveform is assessed by comparing the evaluation times of `TEOBResumSPA` waveforms to that of other FD BNS approximants. In particular, we compare to PN `TaylorF2`, considered here with a 3.5PN-accurate description of the point-mass phasing and 7PN-accurate tidal effects; `IMRPhenomDNRTidal` [59, 60], a phenomenological approximant for aligned-spin binaries augmented by the `NRTidal` phase and amplitude prescriptions; `SEOBNRv4Tsurrogate` [37], a FD surrogate of the EOB tidal model of Ref. [61, 62]; `SEOBNRv4_ROM_NRTidal` a FD reduced-order model of the EOB model [22] augmented by the `NRTidal` phasing.

We simulate the fiducial BNS coalescence with varying initial frequency  $f_0 = (5, 10, 15, 20, 25, 30)$  Hz and uniform frequency spacing  $\Delta f = (1/8192, 1/2048, 1/512, 1/256, 1/128, 1/128)$  Hz, and compute the average generation time to  $f_{\text{max}} = 2048$  Hz over ten repetitions for each of the approximants listed above. The timing results are shown in Fig. 2. `TEOBResumSPA` generation times for  $f_0 \gtrsim 15$  Hz, in green, are comparable to those of `IMRPhenomDNRTidal`, a factor two smaller than `SEOBNRv4_ROM_NRTidal` and up to a factor ten slower than `TaylorF2`. For starting frequencies  $f_0 < 15$  Hz, `TEOBResumSPA` is comparable to `SEOBNRv4Tsurrogate` and `IMRPhenomDNRTidal`, and at least a factor two faster than `SEOBNRv4_ROM_NRTidal`.

Further tests indicate that `TEOBResumSPA` generation times display a small variance over a large parameter

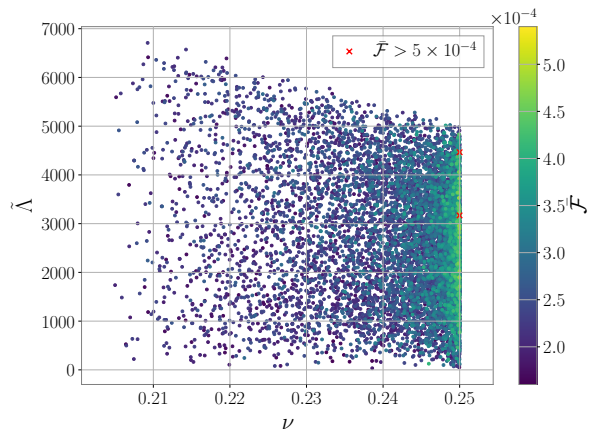
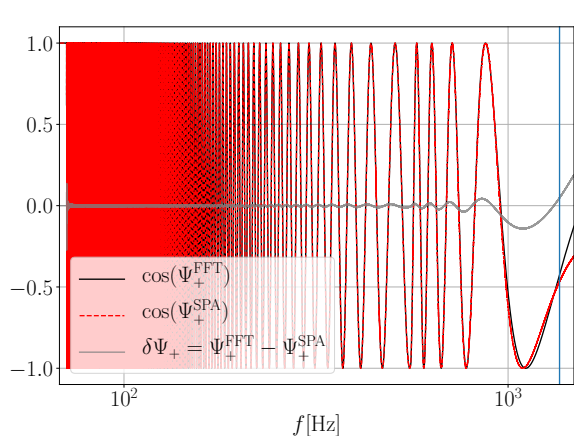


FIG. 1. Left: comparison between the (cosines of) the frequency domain phase of the  $\tilde{h}_+$ , computed with **TEOBResumSPA** and the FFT of **TEOBResumS** for a  $q = 1$ ,  $M = 2.8M_\odot$ ,  $\chi_{1,2} = 0.1$  and  $\tilde{\Lambda} = 400$  system. The phase difference between the two models remains below  $\delta\Psi_+ \lesssim 0.1$  rad to merger (blue vertical line). Right: Unfaithfulness between **TEOBResumSPA** and Fourier-transformed **TEOBResumS**, computed for  $10^4$  binary systems with varying spins, masses and component tidal parameters. Waveforms are computed from an initial frequency of 20 Hz, and matches computed between 20 Hz and 2 kHz. We find that only two values (denoted with red crosses) lie below the SNR 80 threshold of Eq.(4). The mismatch values found, however, are still  $\bar{\mathcal{F}} \sim 10^{-4}$ .

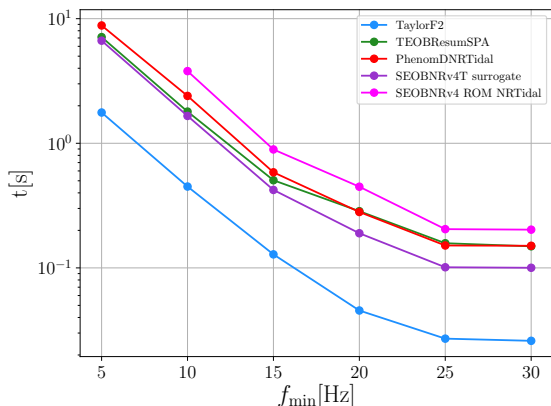


FIG. 2. Generation times of different BNS waveforms averaged over 10 repetitions as a function of initial frequency for a fiducial BNS with  $(M/M_\odot, q, \chi_1, \chi_2, \tilde{\Lambda}) = (2.8, 1, 0, 0, 400)$ . Below 15 Hz **TEOBResumSPA** is comparable to the **SEOBNRv4Tsurrogate** and **IMRPhenomDNRTidal** models and  $\sim 2$  times faster than **SEOBNRv4\_ROM\_NRTidal**.

space ( $m_{1,2} \in [1, 2.5]M_\odot$ ,  $\chi_{1,2} \in [-0.5, 0.5]$ ,  $\Lambda_{1,2} \leq 5000$ ). This is due to the fact that the largest computational burden of the approximant lies in the uniform-frequency interpolation of the multipoles  $h_{\ell m}$ , which is approximately independent of the binary parameters. A further speedup would be simply obtained by considering a non-uniform frequency grid for the likelihood computation, see e.g. [63, 64]. We also stress that, being the SPA analytical, the waveform is valid for any initial frequency and any binary parameters. This is in contrast to wave-

TABLE I. Source properties of GW170817 [65] and GW190425 [66]. The estimates found with **TEOBResumSPA** are compared to the LIGO-Virgo results. The **TEOBResumSPA** analysis is performed up to  $\sim 1$ kHz following [57] in order to minimize waveform systematics; this approach (not the waveform model) is responsible for the slightly different estimate of  $\tilde{\Lambda}$  when compared to [65].

	GW170817		GW190425	
	LVC [65]	<b>TEOBResumSPA</b>	LVC [66]	<b>TEOBResumSPA</b>
$1/q$	0.73-1.00	$0.89^{+0.10}_{-0.2}$	0.8-1.0	$0.9^{+0.1}_{-0.1}$
$\mathcal{M} [M_\odot]$	$1.1975^{+0.0001}_{-0.0001}$	$1.1976^{+0.0001}_{-0.0001}$	$1.4868^{+0.0003}_{-0.0003}$	$1.4868^{+0.0005}_{-0.0005}$
$\tilde{\Lambda}^a$	$300^{+500}_{-190}$	$530^{+350}_{-310}$	$\leq 600$	$\leq 550$
$\chi_{\text{eff}}$	$0.00^{+0.02}_{-0.01}$	$0.00^{+0.02}_{-0.01}$	$0.01^{+0.01}_{-0.01}$	$0.01^{+0.01}_{-0.01}$
$D_L$ [Mpc]	$39^{+7}_{-14}$	$42^{+6}_{-13}$	$159^{+69}_{-72}$	$180^{+61}_{-77}$

<sup>a</sup> The values of  $\tilde{\Lambda}$  are quoted after reweighting to flat in  $\tilde{\Lambda}$  prior. Note however that the procedures followed for the reweighting of the GW170817 and GW190425 posteriors are different, for consistency with Sec. 3D of [65] and App. F.1 of [66].

form models based on surrogates or machine learning, that are limited by the length and parameter range of the training set. Note for example, that it is not possible to generate **SEOBNRv4\_ROM\_NRTidal** waveform at dimensionless frequencies below  $Mf = 9.85 \times 10^{-5}$ , which is the minimal frequency of the surrogate. Thus, the flexibility of the SPA method applied to EOB waveforms has an obvious advantage, in particular in view of the continuous and rapid development of EOB models.

We demonstrate the use of **TEOBResumSPA** in GW parameter estimation by performing the analysis of GW170817 [65, 67–69] and GW190425 [66]. We employ

the `pbilby` [70, 71] and `dynesty` [72] parameter estimation infrastructures and the same setup of [57], to which we refer for all technical details. These analyses run in two-to-three days time on  $4 \times 16$  CPUs. For comparison, the same GW170817 analysis, performed with the `IMRPhenomPv2NRTidal` [29, 60] approximant with an identical setup, required longer than 5 days to complete. Results are listed in Table I, and are consistent with LIGO-Virgo analyses. The measurement of  $\tilde{\Lambda}$  differs from the LIGO-Virgo one because of our conservative choice of the sampling rate, aimed at minimizing high-frequency systematic effects as discussed in [57].

Fast and accurate EOB waveforms will be crucial for the analysis of high-SNR BNS signals as those detectable by the Einstein Telescope or Cosmic Explorer [73–76]. Recent work has demonstrated that at  $\text{SNR} \gtrsim 80$  the systematics among advanced BNS approximants shown in Fig. 2 will be the dominant source of error in the measurements of tidal effects [57]. High-precision measurements for constraining the NS equation of state will require new numerical-relativity informed tidal EOB models [4, 61] or new closed-form representations of the tidal sector [60]. Ongoing work in these directions based on the EOB SPA method will be presented elsewhere.

The EOB SPA waveform can be used to compute accurate inspiral waveforms of intermediate-mass BBH that will be observed by LISA in the mHz to Hz regime [6] and possibly in the dHz regime by planned spaced-based detectors as DECIGO [7, 8, 77]. Beside PN and EOB approximant, no other modeling technique is available for this inspiral-to-late-inspiral regime [78]. We focus on LISA sources with total masses  $\sim 10^3 - 10^5 M_\odot$  and mass ratio up to  $q \sim 80$  [79]. Figure 3 compares  $\sim 10^4$  mismatches between `TEOBResumS`–`TEOBResumSPA` with `TEOBResumS`–`TaylorF2` (at 3.5PN accuracy) computed with the LISA noise curve [80]. The top panel focuses on the  $(\nu, M)$  dependence; the effect of spin is described by  $\chi_{\text{eff}} \equiv S_1/(m_1 M) + S_2/(m_2 M)$ . The figure highlights that `TaylorF2` becomes more and more inaccurate when: (i)  $M \gtrsim 10^3 M_\odot$ ; (ii) when  $q \gtrsim 8$  ( $\nu \lesssim 0.0988$ ) and (iii) when spin magnitudes are not moderate. Specifically, the worst `TEOBResumS`–`TaylorF2` mismatch ( $\bar{\mathcal{F}} = 0.397$ ) corresponds to  $(M/M_\odot, q, \chi_1, \chi_2) = (7670, 55, -0.84, -0.62)$ , and detection losses up to 78%. In addition, we use again Eq. (4), and consider SNR of 20 and 100 [6, 81] to find threshold mismatches of  $\bar{\mathcal{F}}_{20} = 5 \times 10^{-3}$ ,  $\bar{\mathcal{F}}_{100} = 2 \times 10^{-4}$  for  $D = 4$ . `TEOBResumS`–`TEOBResumSPA` mismatches always lie below the lower threshold  $\mathcal{F}_{20}$ , while  $\approx 43\%$  of the simulated signals also satisfy the stricter requirement with  $\bar{\mathcal{F}}_{100}$ . On the contrary, 59% of the PN waveforms are not faithful at SNR 20, and 42% of them correspond to systems with  $q > 8$ . Therefore, `TaylorF2` is not a robust choice for parameter estimation of these BBH sources. The discrepancy between PN and EOB further increases considering higher frequencies; the analysis of intermediate-mass BBH in

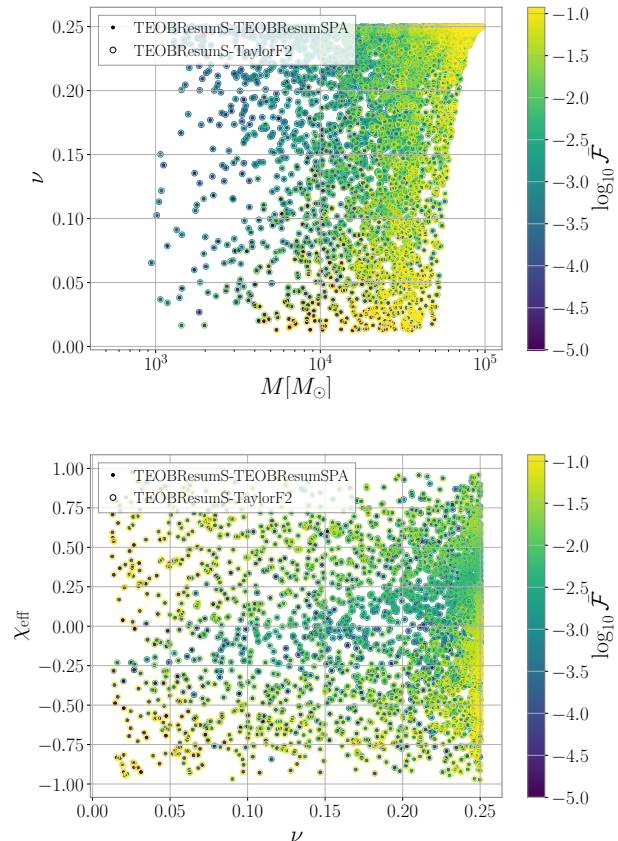


FIG. 3. Mismatches  $\bar{\mathcal{F}}$  between TD `TEOBResumS` and `TEOBResumSPA` or the 3.5PN-accurate `TaylorF2` on the frequency range  $[0.02, 1]$  Hz obtained via Eq. (2) with the LISA noise curve [80]. Top panel: for moderately large mass ratios ( $\nu \leq 0.1$ , corresponding to  $q \gtrsim 7.8$ ) and massive ( $M > 10^4 M_\odot$ ) BBH systems, mismatches between `TEOBResumS` and `TaylorF2` become large, reaching  $\bar{\mathcal{F}} \sim 0.1$ . Bottom panel: `TaylorF2` is effective only for moderate values of the effective spin parameter  $\chi_{\text{eff}} \equiv S_1/(m_1 M) + S_2/(m_2 M)$ .

the the dHz regime (e.g. DECIGO band) will require fast and accurate FD EOB models like `TEOBResumSPA` (see Supplementary Material).

In summary, the EOB SPA method proposed here will crucially support both ground-based and spaced-based observations of long (minutes-to-years) GW transient from compact binaries, whose analysis is a formidable challenge for the years to come.

This work was funded by the Deutsche Forschungsgemeinschaft (DFG) under Grant No. 406116891 within the Research Training Group RTG 2522/1. S. B. acknowledge support by the EU H2020 under ERC Starting Grant, no. BinGraSp-714626. Data analysis was performed on the supercomputer ARA at Jena. We acknowledge the computational resources provided by Friedrich Schiller University Jena, supported in part by

DFG grants INST 275/334-1 FUGG and INST 275/363-1 FUGG. Data postprocessing was performed on the Virgo “Tullio” server in Torino, supported by INFN. TEOBResumS and TEOBResumSPA are both publicly available at

[https://bitbucket.org/eob\\_ihes/teobresums/](https://bitbucket.org/eob_ihes/teobresums/)

This research has made use of data, software and/or web tools obtained from the Gravitational Wave Open Science Center (<https://www.gw-openscience.org>), a service of LIGO Laboratory, the LIGO Scientific Collaboration and the Virgo Collaboration. LIGO is funded by the U.S. National Science Foundation. Virgo is funded by the French Centre National de Recherche Scientifique (CNRS), the Italian Istituto Nazionale della Fisica Nucleare (INFN) and the Dutch Nikhef, with contributions by Polish and Hungarian institutes.

- 
- [1] J. Aasi et al. (LIGO Scientific), *Class. Quant. Grav.* **32**, 074001 (2015), arXiv:1411.4547 [gr-qc].
- [2] F. Acernese et al. (VIRGO), *Class. Quant. Grav.* **32**, 024001 (2015), arXiv:1408.3978 [gr-qc].
- [3] T. Damour, A. Nagar, and L. Villain, *Phys.Rev.* **D85**, 123007 (2012), arXiv:1203.4352 [gr-qc].
- [4] S. Bernuzzi, A. Nagar, T. Dietrich, and T. Damour, *Phys.Rev.Lett.* **114**, 161103 (2015), arXiv:1412.4553 [gr-qc].
- [5] M. Breschi, S. Bernuzzi, F. Zappa, M. Agathos, A. Perego, D. Radice, and A. Nagar, *Phys. Rev.* **D100**, 104029 (2019), arXiv:1908.11418 [gr-qc].
- [6] P. Amaro-Seoane et al. (LISA), (2017), arXiv:1702.00786 [astro-ph.IM].
- [7] M. A. Sedda et al., *Class. Quant. Grav.* **37**, 215011 (2020), arXiv:1908.11375 [gr-qc].
- [8] S. Kawamura et al., (2020), arXiv:2006.13545 [gr-qc].
- [9] A. Sesana, *Phys. Rev. Lett.* **116**, 231102 (2016), arXiv:1602.06951 [gr-qc].
- [10] T. Damour, B. R. Iyer, and B. S. Sathyaprakash, *Phys. Rev.* **D57**, 885 (1998), arXiv:gr-qc/9708034 [gr-qc].
- [11] T. Damour, B. R. Iyer, and B. Sathyaprakash, *Phys.Rev.* **D62**, 084036 (2000), arXiv:gr-qc/0001023 [gr-qc].
- [12] T. Damour, B. R. Iyer, and B. S. Sathyaprakash, *Phys. Rev.* **D63**, 044023 (2001), [Erratum: *Phys. Rev.D72*,029902(2005)], arXiv:gr-qc/0010009 [gr-qc].
- [13] A. Buonanno, B. Iyer, E. Ochsner, Y. Pan, and B. Sathyaprakash, *Phys.Rev.* **D80**, 084043 (2009), arXiv:0907.0700 [gr-qc].
- [14] L. Blanchet, *Living Rev. Relativity* **17**, 2 (2014), arXiv:1310.1528 [gr-qc].
- [15] A. Buonanno and T. Damour, *Phys. Rev.* **D59**, 084006 (1999), arXiv:gr-qc/9811091.
- [16] A. Buonanno and T. Damour, *Phys. Rev.* **D62**, 064015 (2000), arXiv:gr-qc/0001013.
- [17] T. Damour, P. Jaranowski, and G. Schaefer, *Phys. Rev.* **D62**, 084011 (2000), arXiv:gr-qc/0005034 [gr-qc].
- [18] T. Damour, *Phys. Rev.* **D64**, 124013 (2001), arXiv:gr-qc/0103018.
- [19] T. Damour, P. Jaranowski, and G. Schäfer, *Phys.Rev.* **D78**, 024009 (2008), arXiv:0803.0915 [gr-qc].
- [20] T. Damour and A. Nagar, *Phys. Rev.* **D79**, 081503 (2009), arXiv:0902.0136 [gr-qc].
- [21] T. Damour, P. Jaranowski, and G. Schäfer, *Phys. Rev.* **D91**, 084024 (2015), arXiv:1502.07245 [gr-qc].
- [22] A. Bohé et al., *Phys. Rev.* **D95**, 044028 (2017), arXiv:1611.03703 [gr-qc].
- [23] D. Bini, T. Damour, and A. Geralico, *Phys. Rev. Lett.* **123**, 231104 (2019), arXiv:1909.02375 [gr-qc].
- [24] D. Bini, T. Damour, and A. Geralico, *Phys. Rev. D* **102**, 024062 (2020), arXiv:2003.11891 [gr-qc].
- [25] D. Bini, T. Damour, and A. Geralico, *Phys. Rev. D* **102**, 024061 (2020), arXiv:2004.05407 [gr-qc].
- [26] A. Nagar, G. Riemenschneider, G. Pratten, P. Rettegno, and F. Messina, (2020), arXiv:2001.09082 [gr-qc].
- [27] S. Ossokine et al., (2020), arXiv:2004.09442 [gr-qc].
- [28] M. Hannam, P. Schmidt, A. Bohé, L. Haegel, S. Husa, F. Ohme, G. Pratten, and M. Pürrer, *Phys. Rev. Lett.* **113**, 151101 (2014), arXiv:1308.3271 [gr-qc].
- [29] S. Khan, S. Husa, M. Hannam, F. Ohme, M. Pürrer, X. Jiménez Forteza, and A. Bohé, *Phys. Rev.* **D93**, 044007 (2016), arXiv:1508.07253 [gr-qc].
- [30] L. London, S. Khan, E. Fauchon-Jones, X. J. Forteza, M. Hannam, S. Husa, C. Kalaghatgi, F. Ohme, and F. Pannarale, *Phys. Rev. Lett.* **120**, 161102 (2018), arXiv:1708.00404 [gr-qc].
- [31] C. García-Quirós, M. Colleoni, S. Husa, H. Estellés, G. Pratten, A. Ramos-Buades, M. Mateu-Lucena, and R. Jaume, *Phys. Rev. D* **102**, 064002 (2020), arXiv:2001.10914 [gr-qc].
- [32] G. Pratten, S. Husa, C. Garcia-Quiros, M. Colleoni, A. Ramos-Buades, H. Estelles, and R. Jaume, *Phys. Rev. D* **102**, 064001 (2020), arXiv:2001.11412 [gr-qc].
- [33] G. Pratten et al., (2020), arXiv:2004.06503 [gr-qc].
- [34] S. E. Field, C. R. Galley, F. Herrmann, J. S. Hesthaven, E. Ochsner, and M. Tiglio, *Phys. Rev. Lett.* **106**, 221102 (2011), arXiv:1101.3765 [gr-qc].
- [35] M. Pürrer, *Phys. Rev.* **D93**, 064041 (2016), arXiv:1512.02248 [gr-qc].
- [36] B. D. Lackey, S. Bernuzzi, C. R. Galley, J. Meidam, and C. Van Den Broeck, *Phys. Rev.* **D95**, 104036 (2017), arXiv:1610.04742 [gr-qc].
- [37] B. D. Lackey, M. Pürrer, A. Taracchini, and S. Marsat, *Phys. Rev. D* **100**, 024002 (2019), arXiv:1812.08643 [gr-qc].
- [38] R. Cotesta, S. Marsat, and M. Pürrer, *Phys. Rev. D* **101**, 124040 (2020), arXiv:2003.12079 [gr-qc].
- [39] A. Nagar and P. Rettegno, *Phys. Rev.* **D99**, 021501 (2019), arXiv:1805.03891 [gr-qc].
- [40] S. Akcay, S. Bernuzzi, F. Messina, A. Nagar, N. Ortiz, and P. Rettegno, *Phys. Rev.* **D99**, 044051 (2019), arXiv:1812.02744 [gr-qc].
- [41] A. Nagar, F. Messina, P. Rettegno, D. Bini, T. Damour, A. Geralico, S. Akcay, and S. Bernuzzi, *Phys. Rev.* **D99**, 044007 (2019), arXiv:1812.07923 [gr-qc].
- [42] T. Damour, in *Gravitational Radiation*, edited by N. Deruelle and T. Piran (North-Holland, Amsterdam, 1983) pp. 59–144.
- [43] T. Hinderer, *Astrophys.J.* **677**, 1216 (2008), arXiv:0711.2420 [astro-ph].
- [44] T. Damour and A. Nagar, *Phys. Rev.* **D80**, 084035 (2009), arXiv:0906.0096 [gr-qc].
- [45] T. Binington and E. Poisson, *Phys. Rev.* **D80**, 084018 (2009), arXiv:0906.1366 [gr-qc].
- [46] E. E. Flanagan and T. Hinderer, *Phys.Rev.* **D77**, 021502

- (2008), arXiv:0709.1915 [astro-ph].
- [47] T. Damour and A. Nagar, Phys. Rev. **D81**, 084016 (2010), arXiv:0911.5041 [gr-qc].
- [48] M. Favata, Phys.Rev.Lett. **112**, 101101 (2014), arXiv:1310.8288 [gr-qc].
- [49] T. Damour and A. Nagar, Phys.Rev. **D90**, 044018 (2014), arXiv:1406.6913 [gr-qc].
- [50] A. Nagar, G. Riemenschneider, and G. Pratten, Phys. Rev. **D96**, 084045 (2017), arXiv:1703.06814 [gr-qc].
- [51] A. Nagar et al., Phys. Rev. **D98**, 104052 (2018), arXiv:1806.01772 [gr-qc].
- [52] A. Nagar, G. Pratten, G. Riemenschneider, and R. Gamba, (2019), arXiv:1904.09550 [gr-qc].
- [53] S. Bernuzzi, T. Dietrich, and A. Nagar, Phys. Rev. Lett. **115**, 091101 (2015), arXiv:1504.01764 [gr-qc].
- [54] L. Lindblom, B. J. Owen, and D. A. Brown, Phys.Rev. **D78**, 124020 (2008), arXiv:0809.3844 [gr-qc].
- [55] T. Damour, A. Nagar, and M. Trias, Phys. Rev. **D83**, 024006 (2011), arXiv:1009.5998 [gr-qc].
- [56] K. Chatziioannou, A. Klein, N. Yunes, and N. Cornish, Phys. Rev. **D95**, 104004 (2017), arXiv:1703.03967 [gr-qc].
- [57] R. Gamba, M. Breschi, S. Bernuzzi, M. Agathos, and A. Nagar, (2020), arXiv:2009.08467 [gr-qc].
- [58] “LIGO Document T0900288-v3,” <https://dcc.ligo.org/cgi-bin/DocDB/ShowDocument?docid=2974>, Advanced LIGO anticipated sensitivity curves.
- [59] S. Husa, S. Khan, M. Hannam, M. Pürrer, F. Ohme, X. Jiménez Forteza, and A. Bohé, Phys. Rev. **D93**, 044006 (2016), arXiv:1508.07250 [gr-qc].
- [60] T. Dietrich, S. Bernuzzi, and W. Tichy, Phys. Rev. **D96**, 121501 (2017), arXiv:1706.02969 [gr-qc].
- [61] T. Hinderer et al., Phys. Rev. Lett. **116**, 181101 (2016), arXiv:1602.00599 [gr-qc].
- [62] J. Steinhoff, T. Hinderer, A. Buonanno, and A. Taracchini, Phys. Rev. **D94**, 104028 (2016), arXiv:1608.01907 [gr-qc].
- [63] B. Zackay, L. Dai, and T. Venumadhav, (2018), arXiv:1806.08792 [astro-ph.IM].
- [64] S. Vinciguerra, J. Veitch, and I. Mandel, Class. Quant. Grav. **34**, 115006 (2017), arXiv:1703.02062 [gr-qc].
- [65] B. P. Abbott et al. (LIGO Scientific, Virgo), Phys. Rev. **X9**, 011001 (2019), arXiv:1805.11579 [gr-qc].
- [66] B. Abbott et al. (LIGO Scientific, Virgo), Astrophys. J. Lett. **892**, L3 (2020), arXiv:2001.01761 [astro-ph.HE].
- [67] B. P. Abbott et al. (Virgo, LIGO Scientific), Phys. Rev. Lett. **119**, 161101 (2017), arXiv:1710.05832 [gr-qc].
- [68] B. P. Abbott et al. (GROND, SALT Group, OzGrav, DFN, INTEGRAL, Virgo, Insight-Hxmt, MAXI Team, Fermi-LAT, J-GEM, RATIR, IceCube, CAASTRO, LWA, ePESSTO, GRAWITA, RIMAS, SKA South Africa/MeerKAT, H.E.S.S., 1M2H Team, IKI-GW Follow-up, Fermi GBM, Pi of Sky, DWF (Deeper Wider Faster Program), Dark Energy Survey, MASTER, AstroSat Cadmium Zinc Telluride Imager Team, Swift, Pierre Auger, ASKAP, VINROUGE, JAGWAR, Chandra Team at McGill University, TTU-NRAO, GROWTH, AGILE Team, MWA, ATCA, AST3, TOROS, Pan-STARRS, NuSTAR, ATLAS Telescopes, BOOTES, CaltechNRAO, LIGO Scientific, High Time Resolution Universe Survey, Nordic Optical Telescope, Las Cumbres Observatory Group, TZAC Consortium, LOFAR, IPN, DLT40, Texas Tech University, HAWC, ANTARES, KU, Dark Energy Camera GW-EM, CALET, Euro VLBI Team, ALMA), Astrophys. J. **848**, L12 (2017), arXiv:1710.05833 [astro-ph.HE].
- [69] B. P. Abbott et al. (LIGO Scientific, Virgo), Phys. Rev. **X9**, 031040 (2019), arXiv:1811.12907 [astro-ph.HE].
- [70] R. Smith and G. Ashton, (2019), arXiv:1909.11873 [gr-qc].
- [71] I. Romero-Shaw et al., (2020), 10.1093/mnras/staa2850, arXiv:2006.00714 [astro-ph.IM].
- [72] J. S. Speagle, Mon. Not. Roy. Astron. Soc. **493**, 3132 (2020), arXiv:1904.02180 [astro-ph.IM].
- [73] M. Punturo, M. Abernathy, F. Acernese, B. Allen, N. Andersson, et al., Class.Quant.Grav. **27**, 084007 (2010).
- [74] B. Sathyaprakash et al., in *46th Rencontres de Moriond on Gravitational Waves and Experimental Gravity* (2011) pp. 127–136, arXiv:1108.1423 [gr-qc].
- [75] M. Maggiore et al., JCAP **03**, 050 (2020), arXiv:1912.02622 [astro-ph.CO].
- [76] D. Reitze et al., Bull. Am. Astron. Soc. **51**, 035 (2019), arXiv:1907.04833 [astro-ph.IM].
- [77] S. Sato et al., J. Phys. Conf. Ser. **154**, 012040 (2009).
- [78] We recall that Phenomenological approximants are based on fits to PN and EOB waveforms, and do not provide an independent description of this regime.
- [79] Note that we do not simulate coalescences over the entire LISA frequency band, but focus only on the last hours/days of inspiral. This is due to the heavy computational burden represented by interpolating and working with waveforms evaluated on a frequency grid having  $\Delta f \lesssim 1/\text{year}$ .
- [80] T. Robson, N. J. Cornish, and C. Liu, Class. Quant. Grav. **36**, 105011 (2019), arXiv:1803.01944 [astro-ph.HE].
- [81] C. Cutler et al., (2019), arXiv:1903.04069 [astro-ph.HE].
- [82] B. P. Abbott et al. (LIGO Scientific), Class. Quant. Grav. **34**, 044001 (2017), arXiv:1607.08697 [astro-ph.IM].
- [83] M. Punturo, M. Abernathy, F. Acernese, B. Allen, N. Andersson, et al., Class.Quant.Grav. **27**, 194002 (2010).

## Supplemental Material

### STATIONARY PHASE APPROXIMATION (SPA)

We review here the SPA approach to compute the Fourier transform of a signal in the time domain (TD). Given a real TD function  $h(t)$ , defined as

$$h(t) = 2a(t) \cos \phi(t) = a(t)e^{-i\phi(t)} + a(t)e^{i\phi(t)} , \quad (\text{S1})$$

with  $\dot{\phi}(t) \equiv 2\pi F(t) > 0$ , its Fourier transform  $\tilde{h}$  can be expressed as

$$\tilde{h}(f) = \tilde{h}_m(f) + \tilde{h}_p(f) , \quad (\text{S2})$$

where

$$\tilde{h}_m(f) \equiv \int_{-\infty}^{\infty} dt a(t) e^{i(2\pi ft - \phi(t))} , \quad (\text{S3})$$

$$\tilde{h}_p(f) \equiv \int_{-\infty}^{\infty} dt a(t) e^{i(2\pi ft + \phi(t))} . \quad (\text{S4})$$

Since the integrands oscillate rapidly, the largest contribution to the integral comes from the vicinity of the stationary points of their phase (if such points exist). Assuming  $f > 0$ , only the phase of  $\tilde{h}_m$  is stationary and we can therefore neglect the contribution of  $\tilde{h}_p$  to obtain

$$\tilde{h}(f) \simeq \tilde{h}_m(f) \simeq \int_{-\infty}^{\infty} dt a(t) e^{i\psi_f(t)} , \quad (\text{S5})$$

with

$$\psi_f(t) \equiv 2\pi ft - \phi(t) . \quad (\text{S6})$$

Defining the saddle point of  $\psi_f(t)$  as  $t_f$ , we find that the largest contribution to the integral is given by  $F(t_f) = f$ , i.e by points in the Fourier space in which  $f$  equals the instantaneous GW frequency  $F$ . When the second derivative of the phase is non vanishing, one can then estimate Eq. (S5) as

$$\psi_f(t) \simeq \psi_f(t_f) - \pi \dot{F}(t_f) (t - t_f)^2 , \quad (\text{S7})$$

$$a(t) \simeq a(t_f) . \quad (\text{S8})$$

The Gaussian integral one obtains by plugging Eq. (S7) into Eq. (S5) can then be easily solved to obtain

$$\tilde{h}^{\text{SPA}}(f) = \frac{a(t_f)}{\sqrt{\dot{F}(t_f)}} e^{i[\psi_f(t_f) - \pi/4]} . \quad (\text{S9})$$

The above expression can be applied straightforwardly to each mode  $h_{\ell m}$ . The modes are then be combined to obtain the two polarizations as

$$\tilde{h}_+(f) = \frac{1}{2} \sum_{\ell \geq 2} \sum_{m > 0}^{\ell} \tilde{A}_{\ell m}^{\text{SPA}} e^{i\Psi_{\ell m}^{\text{SPA}}} [-2Y_{\ell m}^* + (-)^{\ell} {}_{-2}Y_{\ell - m}] , \quad (\text{S10a})$$

$$\tilde{h}_\times(f) = \frac{i}{2} \sum_{\ell \geq 2} \sum_{m > 0}^{\ell} \tilde{A}_{\ell m}^{\text{SPA}} e^{i\Psi_{\ell m}^{\text{SPA}}} [-2Y_{\ell m}^* + (-)^{\ell+1} {}_{-2}Y_{\ell - m}] . \quad (\text{S10b})$$

The SPA method is applied to the TD waveform generated by `TEOBResumS`, a state-of-the-art effective EOB approximant for spin-aligned binaries [26, 40, 41, 49–53]. Although the procedure is straightforward, we comment on two technical details. First, the SPA implementation requires the evaluation of (second) time derivatives of the phase of each multipole,  $\ddot{\phi}_{\ell m}(t)$ . In order to employ the SPA together with the post-adiabatic approximation of the dynamics [39], we thus implement a fourth-order finite difference formula for non-uniform grids derived in the standard way

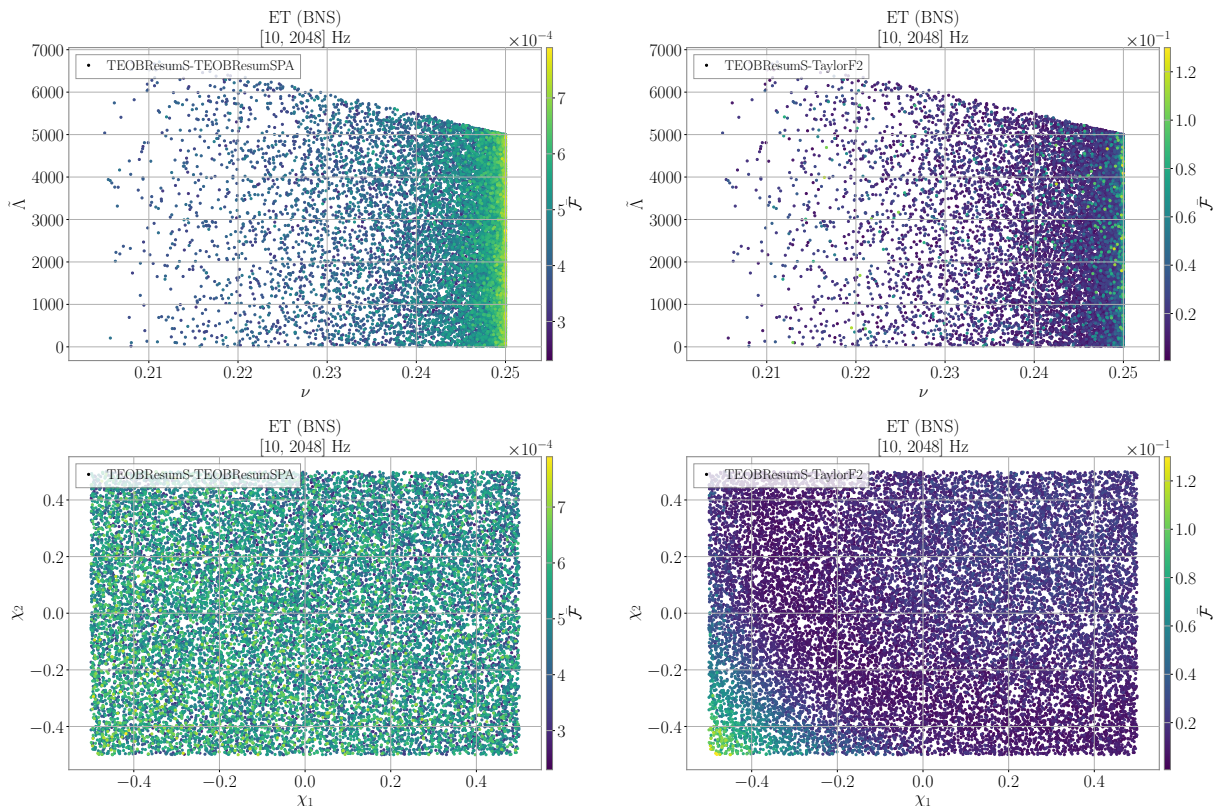


FIG. S1. Mismatches computed between **TEOBResumS** time-domain waveforms and **TEOBResumSPA** or **TaylorF2** for BNS systems between [10, 2048] Hz with the ET noise curve [82]. While **TEOBResumSPA** always displays mismatches better than  $\sim 10^{-4}$ , **TaylorF2** reaches a mismatch of 12% for large misaligned spins (bottom right panel).

using Lagrangian interpolants. A further speed up of the waveform generation can in principle be achieved by substituting the numerical derivatives  $\dot{\phi}_{\ell m}, \ddot{\phi}_{\ell m}$  with their explicit expressions in terms of the EOB dynamical variables. Extensive tests shows that the numerical differentiation is satisfactory (at least for the applications presented in the main paper), and therefore we leave such an improvement to future work.

In general, a direct numerical SPA of the time-windowed modes does not allow for the computation of the FD waveform over the entire frequency range of interest, which from the initial frequency  $f_0$  reaches up to the Nyquist frequency. Moreover, at a given time  $t = \bar{t}$ , the instantaneous frequency of each mode  $f_{\ell m} \equiv \dot{\phi}_{\ell m}(\bar{t})/(2\pi)$  is different for different modes. Therefore, in order to correctly compute the waveform polarizations, it is necessary to: (i) identify a threshold value or frequency  $f_{\ell m}^{\max}$  up to which the SPA maintains its validity and provide a continuation to  $f > f_{\ell m}^{\max}$ , and (ii) interpolate the various modes on a common frequency grid. For BNS systems, the continuation to frequencies higher than merger can be obtained by completing the inspiral-merger model with a FD representation of the postmerger waveform, see e.g. [5]. Alternatively, for inspiral-merger waveforms only, we implement a simple linear extrapolation of the FD phase and a switch off the FD amplitude according to

$$\Psi_{\ell m}(f > f_{\ell m}^{\max}) = \Psi_{\ell m}(f_{\ell m}^{\max}) + \Psi'_{\ell m}(f_{\ell m}^{\max})(f - f_{\ell m}^{\max}), \quad (\text{S11})$$

$$\tilde{A}_{\ell m}(f > f_{\ell m}^{\max}) = \tilde{A}_{\ell m}(f_{\ell m}^{\max}) \left( \frac{f_{\ell m}^{\max}}{f} \right)^{10/3}, \quad (\text{S12})$$

where  $f_{\ell m}^{\max} \equiv f_{\ell m}(t_{\max})$  and  $t_{\max}$  is defined as the time when  $\ddot{f}_{\ell m} = 0$ . This choice of  $t_{\max}$  and  $f_{\ell m}^{\max}$  ensures that, when considering the  $\ell = m = 2$  mode, we also capture part of the frequency evolution *beyond* merger, as  $f^{\text{mrg}} < f_{22}^{\max}$ . The interpolation on the common grid is performed after the extension to high frequencies on a uniformly spaced interval, whose  $\Delta f$  is user-input. In GW parameter estimation,  $\Delta f$  would be equal to the inverse of the length of the segment analyzed.

A C implementation of **TEOBResumS** and **TEOBResumSPA** with a python interface is publicly available at

[https://bitbucket.org/eob\\_ihes/teobresums/](https://bitbucket.org/eob_ihes/teobresums/)



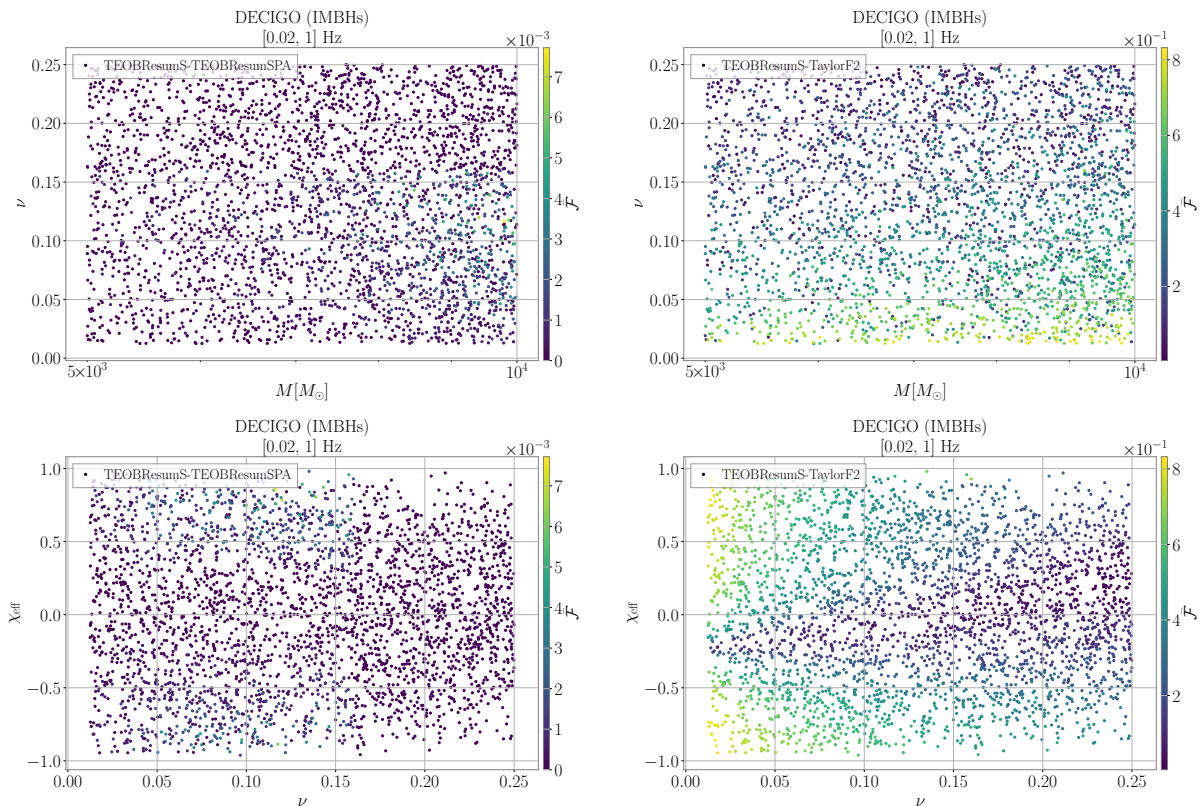


FIG. S2. Mismatches computed between TEOBResumS time-domain waveforms and TEOBResumSPA or 3.5PN accurate TaylorF2 for heavy IMBH systems in the frequency window  $[0.02, 1]$  Hz of the DECIGO noise curve [77]. We use the effective spin parameter  $\chi_{\text{eff}} \equiv S_1/(m_1 M) + S_2/(m_2 M)$ . The large mismatches between TEOBResumS and TaylorF2 clearly demonstrate that the latter is not even effectual for describing heavy asymmetric IMBH systems in the DECIGO frequency band.

## EOB-SPA FAITHFULNESS FOR BNS AND IMBH SYSTEMS IN VARIOUS FREQUENCY BANDS

In this Section we collect additional mismatch studies to complement those reported in the main text. We focus on: (i) BNS waveforms in the frequency window of the Einstein Telescope (ET) [74, 75, 83] (BNS,  $f \in [10, 2048]$  Hz) and (ii) Intermediate mass black holes (IMBHs) in the DECIGO [8, 77] frequency range. In particular, we consider light IMBHs (L-IMBHs) with  $q \in [1, 80]$ ,  $M/M_\odot \in [100, 5000]$ , and frequency range  $f \in [0.02, 10]$  Hz, and heavy IMBHs, with  $M/M_\odot \in [5000, 10000]$  and frequency range  $f \in [0.02, 1]$  Hz.

### BNS waveforms in the ET band

Figure S1 displays the mismatches between TEOBResumS and TEOBResumSPA (left panels) and TEOBResumS and the 3.5PN-accurate TaylorF2 (right panels), computed using the theoretical ET [74, 75, 83] noise curve [82]. We consider BNS systems with  $m_{1,2}/M_\odot \in [1., 2.5]$ ,  $\chi_{1,2} \in [-0.5, 0.5]$  and  $\Lambda_{1,2} \in [10, 5000]$ , and compute the mismatches from 10 Hz to 2048 Hz. Noticeably, while TEOBResumS – TEOBResumSPA mismatches are of  $\mathcal{O}(10^{-4})$ , TEOBResumS–TaylorF2 differences can exceed 10% for binaries with large negative spins. The largest mismatch ( $\bar{\mathcal{F}} = 0.13$ ) is obtained with a system of  $(M/M_\odot, q, \chi_1, \chi_2, \tilde{\Lambda}) = (4.9, 1.02, -0.48, -0.5, 4089)$ . This value corresponds to a threshold SNR of 5, which lies below the detection threshold SNR, nominally taken to be  $\text{SNR}_{\text{det}} = 8$ . In general TaylorF2 is found to get progressively inaccurate as the magnitude of the anti-aligned spins is increased. This implies that the use of the standard 3.5PN-accurate TaylorF2 for GW searches can lead to detection losses up to  $\sim 34\%$  when considering very extreme BNS systems.

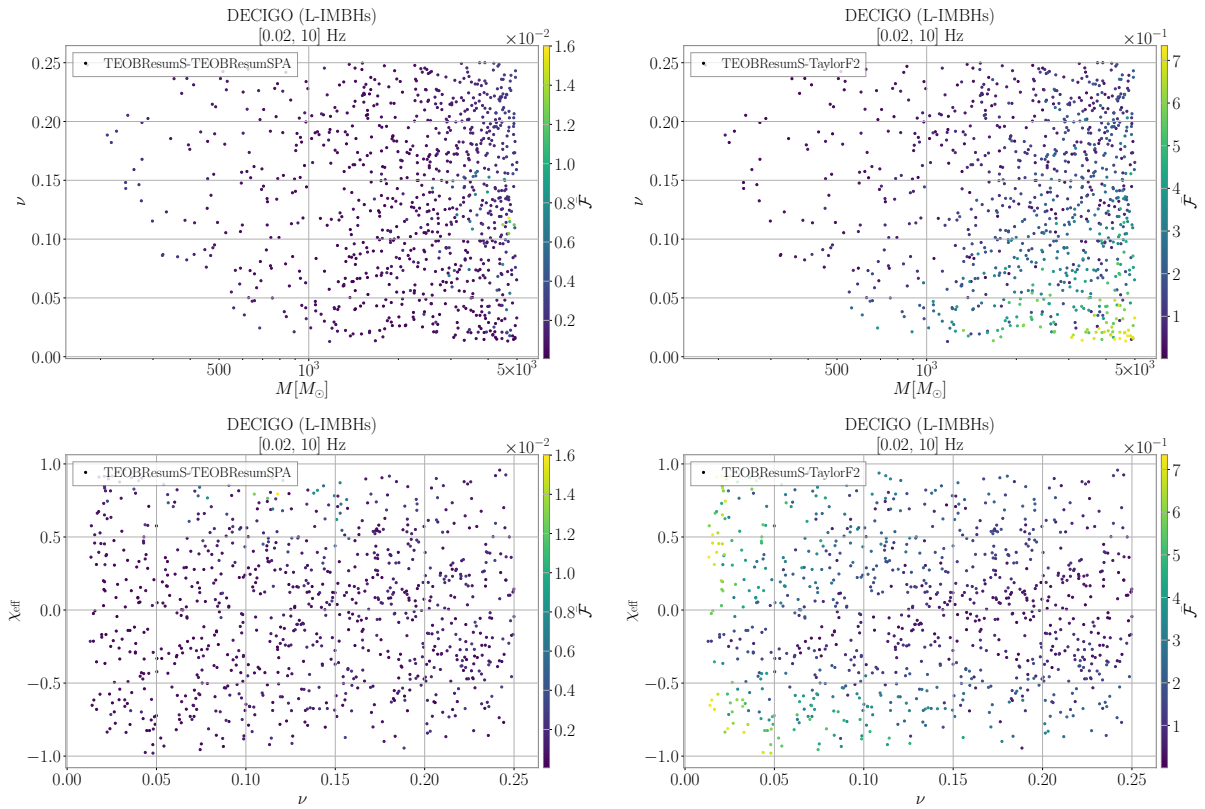


FIG. S3. Mismatches computed between TEOBResumS time-domain waveforms and TEOBResumSPA or 3.5PN-accurate TaylorF2 for light IMBH systems in the frequency window  $[0.02, 10]$  Hz of the DECIGO noise curve [77]. We use the effective spin parameter  $\chi_{\text{eff}} \equiv S_1/(m_1 M) + S_2/(m_2 M)$ . The large mismatches between TEOBResumS and TaylorF2 clearly demonstrate that the latter is not even effectual for describing light asymmetric IMBH systems in the DECIGO frequency band.

### IMBHs waveforms in the DECIGO band

Let us finally turn to considering the DECIGO detector [8, 77]. We compute mismatches for heavy IMBHs, having  $q \in [1, 80]$  and  $M/M_{\odot} \in [5000, 10000]$  in the frequency range  $f \in [0.02, 1]$  Hz, and light IMBHs, having  $M/M_{\odot} \in [100, 5000]$  in the range  $f \in [0.02, 10]$  Hz. The results are collected in Figs. S2 and S3. Unsurprisingly, the largest differences are found for heavy systems with large mass ratios. The mismatches computed in the  $[0.02, 1]$  Hz band are larger than the ones found with LISA, as DECIGO is expected to be more sensitive in that regime. We find that TEOBResumS – TEOBResumSPA mismatches are of  $\mathcal{O}(10^{-4})$ , with few exceptions reaching up to  $\mathcal{O}(10^{-2})$ . TEOBResumS–TaylorF2 mismatches, instead, can grow as large as 80% for binaries with large spins and high mass ratio. This value corresponds to potential detection losses of 99% of the systems having such properties.